Temporal changes in seismic velocity of the crust around Iwate volcano, Japan, as inferred from analyses of repeated active seismic experiment data from 1998 to 2003

Takeshi Nishimura[1], Satoru Tanaka[1], Teruo Yamawaki[1], Hidekazu Yamamoto[2], Takashi Sano[2], Minemori Sato[1], Hisashi Nakahara[1], Naoki Uchida[1], Shuichiro Hori[1], and Haruo Sato[1]

[1]*Graduate School of Science, Tohoku University, Sendai 980-8578, Japan*
[2]*Faculty of Engineering, Iwate University, Morioka 020-8551, Japan*

We have examined temporal changes in seismic velocity of the crust through repeated active seismic experiments at Iwate volcano, Japan, where a significant volcanic activity and an M6.1 earthquake were observed in 1998. We apply a cross spectrum moving window technique to seismic data recorded at eight stations for the six explosions detonated from 1998 to 2003. The seismic velocity at the frequency range of 3–9 Hz decreased by about 1% during the three months including the occurrence of M6.1 earthquake. The seismic velocity gradually increased, and about one third of the decrease was recovered by 2002. Then, the seismic velocity decreased again in 2003. Spatio-temporal changes in the volumetric strains predicted from the M6.1 fault mechanism and the volcanic pressure sources are well correlated with the seismic velocity changes observed in 1998. However, the predicted stress fields are not completely matched with the observed velocity changes from 1998 to 2003. This inconsistency may be due to unknown regional tectonic stress field and/or localized stress fields induced by volcanic pressure sources. It should be noted that the observed velocity changes indicate frequency dependent characteristics although the mechanism is not yet understood.

Key words: Temporal changes, seismic velocity, Iwate vocano, active seismic experiment.

1. Introduction

Temporal changes of the crustal structure have been a major topic of the solid earth, and many seismologists have attempted to detect a small change of the structure associated with seismic and volcanic activities. For example, Poupinet *et al*. (1984) showed that the seismic velocity around the hypocentral area of the Coyote Lake earthquake (M5.9) decreased down to 1% by applying a cross spectrum method to multiplet seismic events. He and his colleagues further examined temporal changes of shallow structure at Merapi volcano and reported a 1% increase of seismic velocity several months before the 1992 eruption (Poupinet *et al*., 1996; Ratdomopurdo and Poupinet, 1995). Furumoto *et al*. (2001) examined the first arrival time data of repeated active seismic experiments at Izu Oshima, Japan, which have been planned by Geological Survey of Japan for monitoring the structure around the focal zone of a future Tokai earthquake. By correcting tidal effects in the arrival times, they succeeded in estimating the rate of velocity change to be 0.1% per year, which originates from stress accumulation due to the subducting Philippine plate. Baish and Bokelmann (2001) showed a recovery of the heterogeneity in the crust near the M.6.9 Loma Prieta earthquake by analyzing waveform similarities of multiplet earthquakes. *S*-wave splitting waves and coda-*Q* analyses have succeeded

in detecting a small change of the structure around active seismic areas (e.g., Hiramatsu *et al*., 2000; Saiga *et al*., 2003; Tadokoro and Ando, 2002). Repeated seismic reflection measurements in the Kakkonda geothermal area also found structure changes around micro-seismic zones (Matsushima *et al*., 2004). These previous studies indicate that temporal changes of the crustal structure are related with seismic/volcanic activities and plate motions.

Iwate volcano, which is a strato volcano located in the middle of north eastern Japan, have been active since the end of 1997. Significant volcanic earthquakes and crustal deformation have been detected by dense seismic and geodetic observations around the volcano (Tanaka *et al*., 2002b; Miura *et al*., 2000). Although the volcano did not erupt, on September 3, 1998, a large earthquake with a magnitude of 6.1 hit Shizukuishi-town that is located south west of the summit of the volcano (Nakahara *et al*., 2002). Nishimura *et al*. (2000b) and Uchida *et al*. (2002) analyzed the seismic waves excited by two active experiments that were carried out one month before and two months after the M6.1 earthquake, and showed velocity decrease of about 1% in the upper crust. Nakamura *et al*. (2002) also indicated 1% velocity decrease in the seismic velocity from analyses of direct *P*-waves observed at permanent stations of Tohoku University, and Matsumoto, S. *et al*. (2001) reported a change of heterogeneous structure around the hypocenter of the M6.1 earthquake on the basis of coherence analyses of seismic array data.

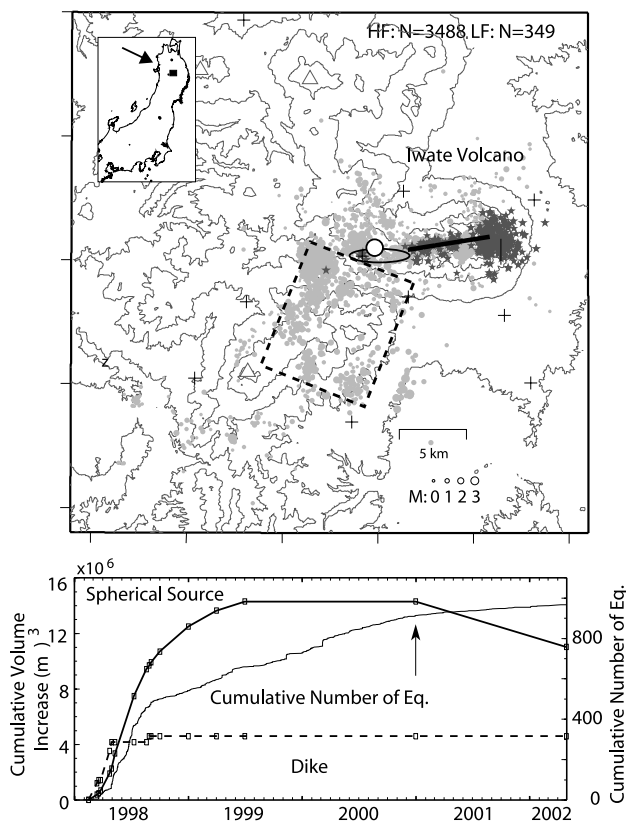To examine whether the crustal structure around the M6.1

Fig. 1. (a) Seismic and volcanic activities around Iwate volcano. Epicenters of volcano tectonic earthquakes and low-frequency earthquakes are indicated by gray circles and dark grey stars, respectively. Source region of very long period seismic events (Nishimura *et al.*, 2000a) are indicated by an open ellipse, and locations of spherical volumetric sources and dikes inferred from geodetic measurements (Miura *et al.*, 2000; Tohoku Univ., 2003) are denoted by a large open circle and thick lines, respectively. M6.1 fault zone estimated from co-seismic displacement (Miura *et al.*, 2000) is also projected on the horizontal plane (broken line). (b) Temporal changes of cumulative number of earthquakes (thin line), cumulative volumes of spherical volumetric sources (thick line) and dike (broken line).
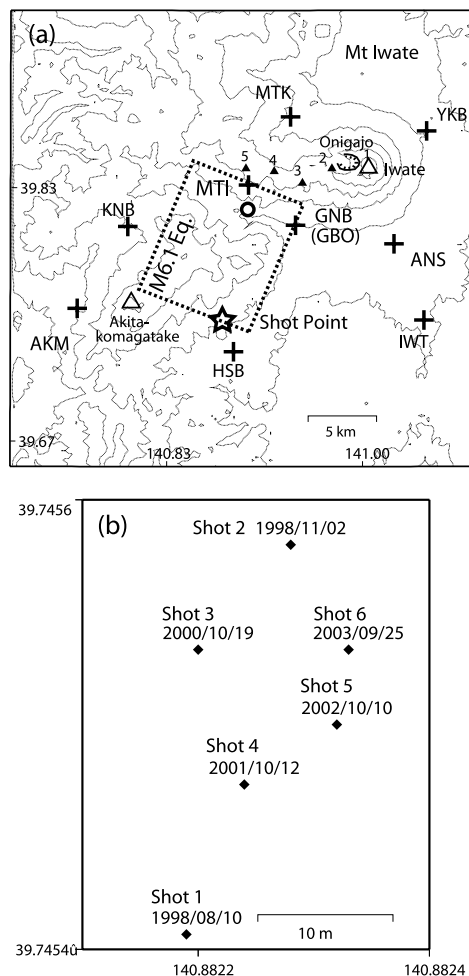

Fig. 2. (a) Location map of seismic stations (large plus symbols), explosion-point (star), the epicenter of the M6.1 earthquake (solid circle). Horizontal projection of the M6.1 fault plane is indicated by a rectangular of broken line. Peaks 1 to 5 of Iwate volcano (solid triangles) are aligned in the east-west direction. Peak 1 is the summit (2036 m), Yakushidake. Peaks 2, 3, 4, and 5 are Kurokura, Ubakura, Ohmatukura and Mitsuishi, respectively. (b) Close-up of locations of six explosion points.

earthquake and Iwate volcano recovers the seismic velocity decrease or not, we further conducted same active experiments from 2000 to 2003. In the present study, we analyze seismic data of active seismic experiments for six years from 1998 to 2003, during which the M6.1 earthquake took place and Iwate volcano experienced significant activities. First, we briefly summarize the volcanic and seismic activities around Iwate volcano as well as outlines of the active experiments. We apply the moving window cross spectrum technique presented by Poupinet *et al.* (1984) to the seismograms of repeated seismic active experiments in order to evaluate small changes in seismic velocity of the crust. In addition, we examine the wave properties by using semblance analyses to seismic array data. Finally, we compare the estimated velocity changes with the deformation field that is precisely determined from geodetic data observed around the volcano for understanding the origins of the velocity changes.

2. Activity of Iwate Volcano and M6.1 Earthquake

Figure 1 summarizes spatial distribution of volcanic and seismic activities of Iwate volcano. In September 1995,

notable volcanic tremor was first observed. At the end of 1997, small changes were detected in records of borehole tilt and strain meters at YKB, ANS and GNB stations that are deployed on the flank of the volcano. Earthquake swarms occurred in March 1998, and then volcanic earthquakes, low-frequency earthquakes, very long period seismic events and tremor gradually became active at a shallow part of the volcano (Nishimura *et al.*, 2000a; Tanaka *et al.*, 2002b). And also, deep low-frequency earthquakes became active around the Moho discontinuity (Nakamichi *et al.*, 2003). Borehole tilt and strain meters and the global positioning system (GPS) networks deployed around the volcano detected ground deformations, from which spherical volumetric sources and east-west oriented dikes were inferred (Miura *et al.*, 2000; Tohoku Univ., 2003). These seismic and ground deformation activities were most prominent from April to June in 1998.

On September 3, 1998, an M6.1 earthquake took place on the south west of the summit of Iwate volcano. The hypocenter is located closely at the spherical volumetric

Table 1. Information of the six artificial explosions.

Shot Number	Date	Time	Depth (m)	Dynamite charge (kg)
1	Aug. 10, 1998	00 h 52 m 08 s	30	100
2	Nov. 2, 1998	00 h 02 m 03 s	30	100
3	Oct. 19, 2000	01 h 22 m 00 s	50	200
4	Oct. 12, 2001	01 h 12 m 00 s	30	100
5	Oct. 10, 2002	01 h 07 m 00 s	30	100
6	Sep. 25, 2003	01 h 12 m 02 s	30	100

sources detected by the geodetic measurements (Tanaka *et al.*, 2002b; Umino *et al.*, 1998). The earthquake is a reverse fault dipping to the west (a dip of 41 degree and a strike of 216 degree; Earthquake Information Center, Univ. of Tokyo, 1998), and a part of the fault reached the ground surface at the northeastern part of the focal area (Koshiya and Ohtani, 1999). The total moment release is estimated to be 3.9×10^{17} Nm by a waveform inversion of strong motion data, and large slips are observed at the shallow parts of the reverse fault (Nakahara *et al.*, 2002). Analyses of the GPS network data indicate that the reverse fault averagely slipped 0.37 m on the fault plane of 6 km × 10 km with a strike of 203 degree, a dip of 35 degree and a rake of 117 degree (Miura *et al.*, 2000).

Since the occurrence of the M6.1 earthquake, the volcanic activity gradually declined and did not show remarkable increases in ground deformation and seismic activities. In March 1999, however, some noticeable surface activities were observed: enlargement of the area adhered by sulfur at the bottom of the Onigajo caldera, new appearance of dead plants at the western edge of the caldera, and formations of new fumeroles along the peaks of Kurokura and Ubakura (peaks 2 and 3 in Fig. 2). These anomalies on the ground surface appeared at once over 5.5 km long of the east-west direction on Iwate volcano (including Onigajo caldera and peaks 2 to 5 in Fig. 2), and have been observed at least until 2002 (Doi, 2002). In the latter part of 2000, the volcano began to deflate, and about 20% of the inflation caused in 1998–2000 had been recovered by the middle of 2002 (Geographical Survey Institute, 2003; Tohoku Univ., 2003).

3. Active Seismic Experiments and Data

Figure 2 shows a location map of artificial explosion sites (shot points), seismic stations, the fault area of the M6.1 earthquake, and peaks of Iwate volcano. The shot points are located near the south edge of the M6.1 fault. The six shot points are close to each other in an area of 30 m × 10 m (Fig. 2(b)). The first and second artificial explosions were detonated on August 10 and November 2, 1998, respectively, which were about one month before and two months after the M6.1 earthquake, by the Research Group for Inland Earthquakes and the Research Group for Exploration Seismology, Japan. About two years later, the third explosion was conducted on October 19, 2000, as a part of the volcano seismic exploration program under the auspices of the National Project of Prediction for Volcanic Eruptions in Japan (Tanaka *et al.*, 2002a). From 2001 to 2003, we carried out explosions three times every year with a support of a scientific grant of MEXT, Japan. To generate near identi-
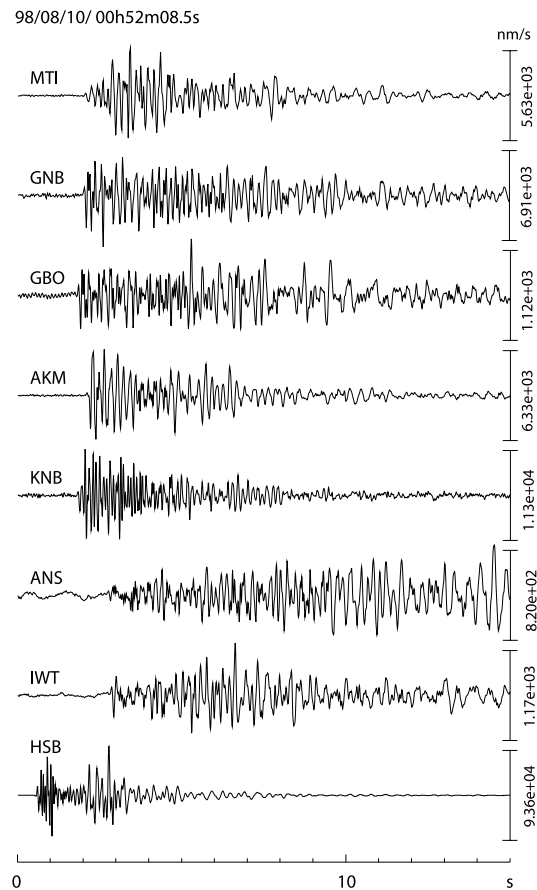

Fig. 3. Vertical velocity seismograms recorded at eight stations for shot 1. The records of broadband seismometer (GNB, MTI) are bandpass filtered from 1 to 16 Hz. The starting time of the seismograms is labeled on the top of the figure.

cal seismic waves, we carefully unified the explosion style except the location of shot points. We used a chemical explosion of 100 kg dynamite embedded at a depth of 30 m for each experiment. However, only for the 3rd experiment in 2000, a source of 200 kg dynamite at a depth of 50 m was used to generate larger seismic waves because the main purpose of the 3rd experiment was the investigation of 3-D seismic structure of Iwate volcano (Tanaka *et al.*, 2002a). Table 1 summarizes information on these six shots.

For six of the explosions, we obtained high-quality waveform data at stations around Iwate volcano: MTI, GNB, AKM, KNB, HSB, ANS and IWT stations. GNB, AKM, HSB, ANS and IWT stations are permanent stations of the Research Center for Prediction of Earthquakes and Volcanic Eruptions (RCPEV) of Tohoku University. MTI and KNB
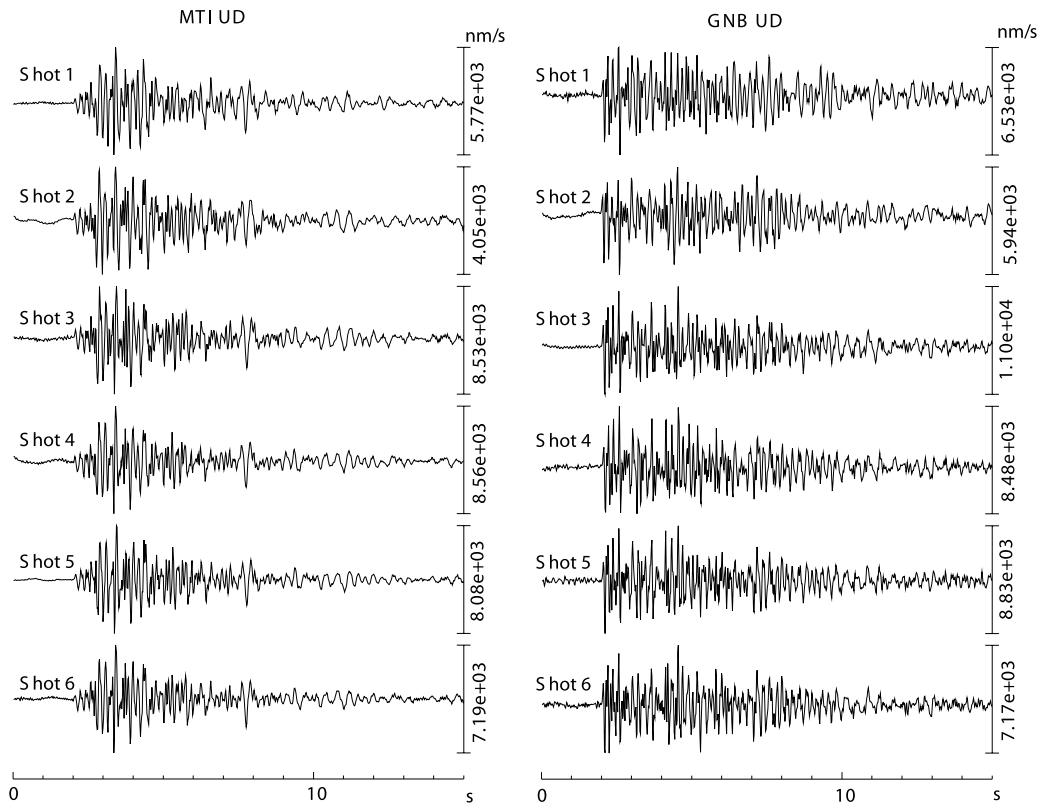
Fig. 4(a). Vertical velocity seismograms at MTI and GNB stations for the six shots.

stations are temporally deployed on the mountain flank to record volcanic earthquakes associated with the activity of Iwate volcano (Nishimura *et al.*, 2000a; Tanaka *et al.*, 2002b). Two broadband seismometers of STS-2 (Strecke-sen) were installed at MTI and GNB stations, and their signals were digitized at each site with a sampling rate of 0.02 s and an A/D resolution of 24 bit by a portable data logger of LS8000WD (Hakusan Co.). The internal clock (precision is higher than 10^{-6}) was corrected by a GPS clock system every two hours so that error of the recording time was less than 8 ms. Since the 3rd experiment, signals of the broadband seismometer at GNB station are continuously digitized with a sampling rate of 0.01 s and an A/D resolution of 22 bit by OT4100 (Oki Electronics) and are transmitted to a data acquisition system at RCPEV through a telephone line. Since sampling rates of the signals at GNB station are not the same, we re-sampled the records at a rate of 0.02 s after filtering the seismograms from 1 to 16 Hz for the 3rd to 6th experiments. GNB station is also equipped with a bore-hole three-component short-period (1 s) seismometer at a depth of 300 m. Same borehole seismometers are used at ANS and HSB stations. Three-component short-period (1 s) seismometers are installed at a base on horizontal vault at IWT and AKM stations, and are embedded in soil at KNB station. These signals from short-period seismometers at GNB, ANS, IWT, AKM, HSB and KNB stations are digitized with a sampling rate of 0.01 s and an A/D resolution of 12–22 bit, and then the data are transmitted to RCPEV in real time. The code GBO denotes the records of borehole short period seismometer at GNB to discriminate it from the broadband seismograms. We call the six explosions shot 1,

shot 2 and so on.

Figure 3 shows an example of the seismograms of vertical component observed at the eight stations for shot 1. The signals of broadband seismometers are bandpass filtered from 1 to 16 Hz to eliminate long-period noises. We use three component data at the eight stations for the following analysis, but do not use shot 5 data of KNB station and shot 6 data of HSB station, which were not working during the experiments.

4. Cross Spectrum Analyses

If the seismic velocity of the crustal structure temporally changes for the observation periods, the seismic waves excited by shot 1 are expected to be different in travel time from those by the following five shots. The travel times of first arrivals of each shot may provide us an accurate estimate of the seismic velocity, but the time accuracy of MTI station is not enough to resolve a small change (ca. 1%) of the seismic velocity. Therefore, to extract a small difference in travel times of the waveforms for two shots, we apply the cross spectrum moving window technique proposed by Poupinet *et al.* (1984), by which time difference can be precisely estimated even if absolute recording times are not so accurate. We do not examine the first arrivals of direct *S* wave, because *S* wave is ambiguous.

4.1 Phase change

Coherence and phase difference as a function of time are calculated by shifting a time window every 0.1 s from the explosion time. Length of the time window is set at 1.0 s. The coherence and phase difference are estimated for the 9 frequencies from 3.1 Hz to 9.2 Hz (3.1 Hz, 3.9 Hz, 4.7
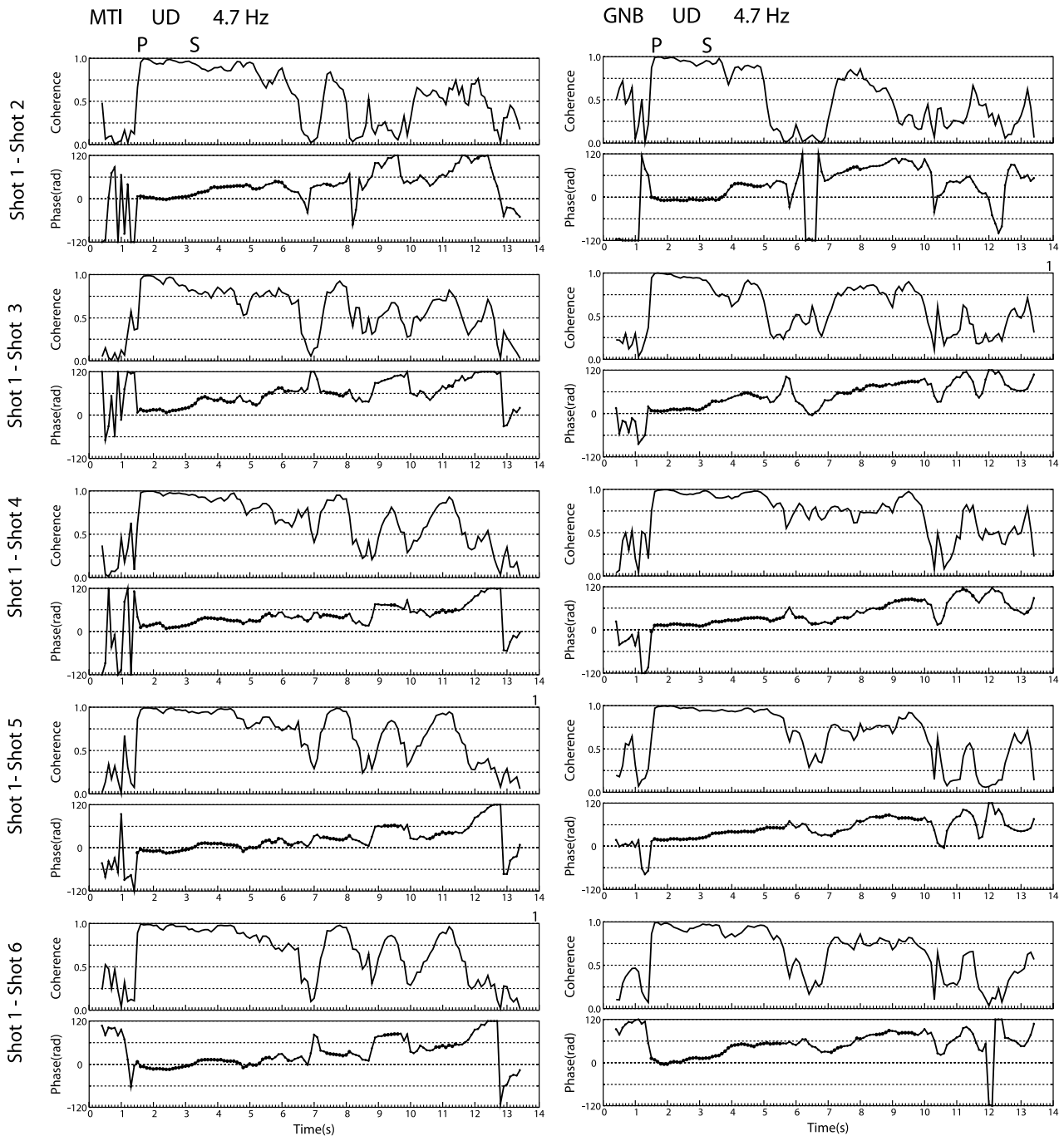
Fig. 4(b). Time sequence of coherence and phase difference of MTI and GNB stations at the frequency of 4.7 Hz. Positive values in phase difference, ϕ, indicate phase delays in waveform of shot 2–6 to shot 1. The data having coherence larger than 0.75 are marked by small solid circles. Arrival times of P and S-waves are denoted by symbols of P and S, respectively, on the top trace for each station. Arrival times of S-waves are calculated by assuming $Vp/Vs = 1.73$.

Hz, 5.5 Hz, 6.2 Hz, 7.0 Hz, 7.8 Hz, 8.5 Hz and 9.2 Hz). The waveforms sometimes show low signal to noise ratios below 3 Hz at several stations, so we do not use the frequency components lower than 3 Hz. Figure 4(a) shows vertical components of the seismograms recorded at MTI and GNB stations for shots 1–6. The time axes for the six seismograms are adjusted by eye-picked arrival times of initial phase. Time series of coherence and phase difference at 4.7 Hz for the shot 1 data to the other shots are plotted in Fig. 4(b). For both of the stations, the coherences for each pair of the shots show large values of more than 0.75 for

several seconds just after the P-arrivals. These high coherence signatures suggest that the six artificial explosions excited nearly equal seismic waves. Although the coherences sometimes indicate significant dips, large values continue from the P-wave arrival to lapse time of about 8–10 s for most of the pairs. In Fig. 4(b), a positive value of the phase difference represents a phase delay of the waveforms of shots 2–6 to those of shot 1. It is found that the phase difference ϕ for the pair of shot 1 to shot 2 gradually increases with lapse time when we place the focus on the portions having large coherence. Similar characteristics are
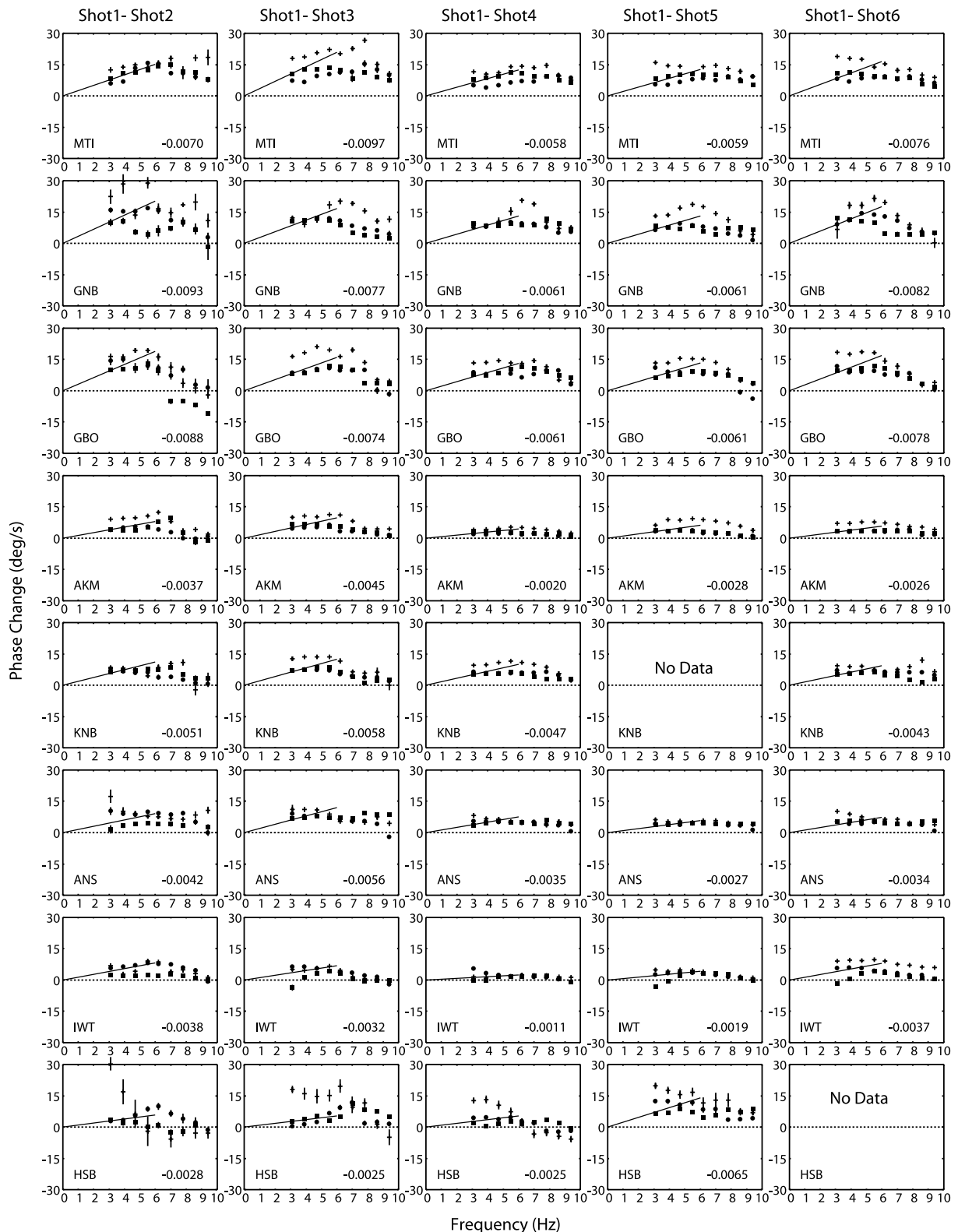
Fig. 5. Frequency dependence of the time derivative of phase difference, $d\phi/dt$. Solid circles, squares, and plus symbols represent $d\phi/dt$ estimated from the data of UD, NS, and EW components, respectively. Fine line is the best fit line for the velocity change at 3–6 Hz that is shown at the bottom right at each panel (see text).

also recognized for horizontal components at these stations (not shown in figure). This result implies that the seismic velocity of the structure at this frequency range decreased for the period between August 1998 (shot 1) and November 1998 (shot 2), during which the M6.1 earthquake took place. The phase differences for the pairs of shots 1–3, 1–4, 1–5 and 1–6 also gradually increase with lapse time.

Closely looking at Fig. 4, we find a jump in time series of the phase difference. For example, for shot 1–2 at GNB station, the phase difference suddenly increases about 40 deg
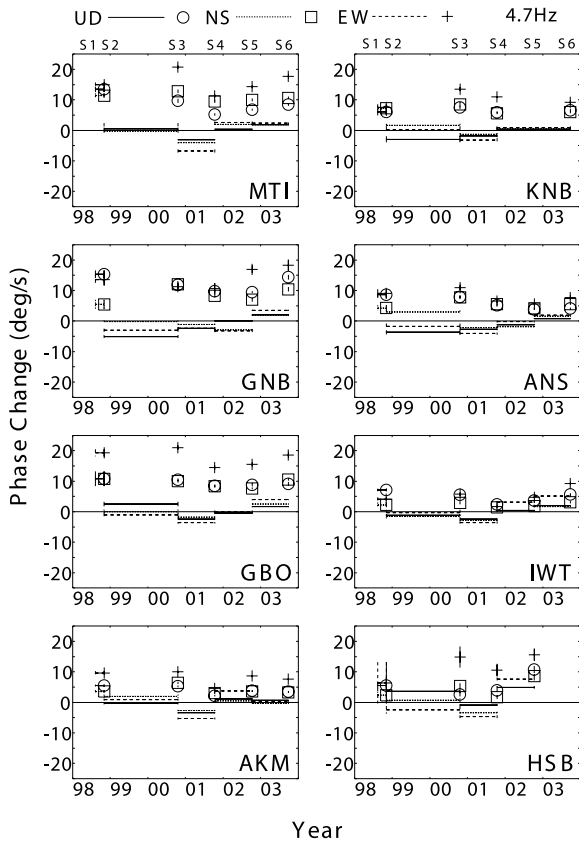
Fig. 6. Temporal variations of the phase change at 4.7 Hz for the six years from 1998 to 2003. Open circles, squares and plus symbols represent the phase changes of UD, NS EW components, respectively, for the pairs of shot 1 to the other shots. Horizontal lines represent the phase changes estimated for the pairs of consecutive shots. Vertical lines indicate one standard deviation. Time window of 10 s is used for fitting a straight line to the phase changes with lapse time.
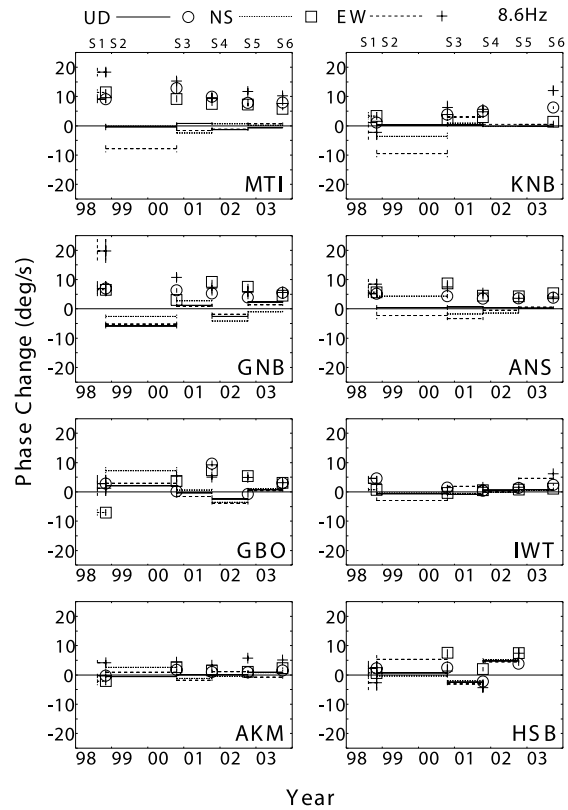
Fig. 7. Temporal variations of the phase change at 8.6 Hz. The others are the same as Fig. 6.
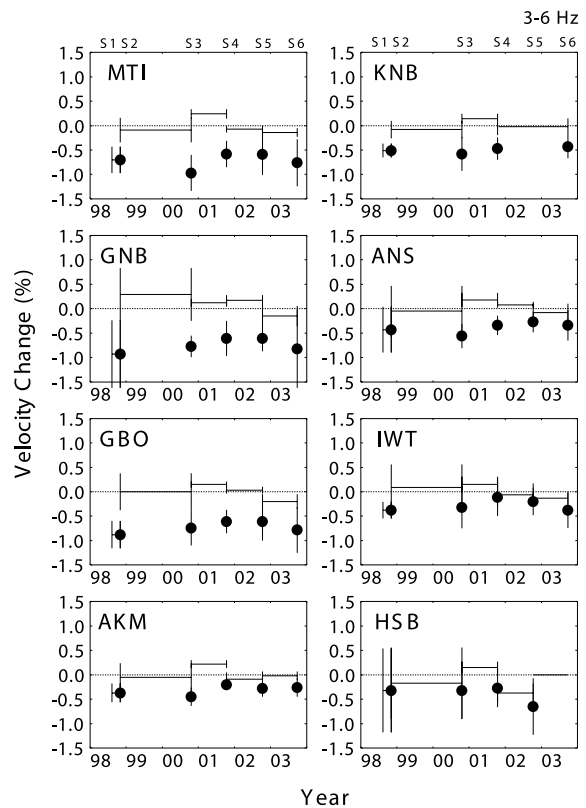

Fig. 8. Temporal changes of seismic velocity at 3–6 Hz for the six years from 1998 to 2003. Solid circles represent the velocity changes estimated for the pairs of shot 1 to the other shots. Horizontal lines represent the phase changes estimated from the pairs of consecutive shots. Vertical lines indicate one standard deviation. Time window of 10 s is used for fitting a straight line to the phase changes with lapse time.

(see at about 4 s in Fig. 4(b)) although the phase difference is constant from *P*-wave to *S*-wave arrivals. Such changes in phase difference may be related with a localized change of the structure and/or difference of phase types such as *P*-, *S*- and surface waves (Poupinet *et al.*, 1996). However, these rapid changes are not systematically found for all pairs of shot 1 to the other shots. Hence, in the present study, we evaluate an average feature of the structure from the waveforms for 10 s from the *P*-wave arrivals, and measure the time derivative of the phase differences, $d\phi/dt$, by fitting a straight line (hereafter we call $d\phi/dt$ phase change). In Fig. 5, the phase changes $d\phi/dt$ are plotted for the five pairs of shot 1 to the other shots. For each pair and each station, the phase changes of the three components are shown from 3.1 Hz to 9.2 Hz. The phase changes for the pair of shot 1–2 are generally larger than those for the other pairs (shot 1–3, shot 1–4, shot 1–5, and shot 1–6). Most of the stations show that, at the frequencies less than about 6 Hz, the phase changes almost linearly increases with frequency. On the other hand, at the frequencies larger than 6 Hz, the phase changes become constant or even decrease with increasing frequency. Although the mechanism causing such frequency dependence is not known, it is noteworthy to mention that the phase change (i.e., fractional change of the seismic velocity) of the crust is dependent on the fre-
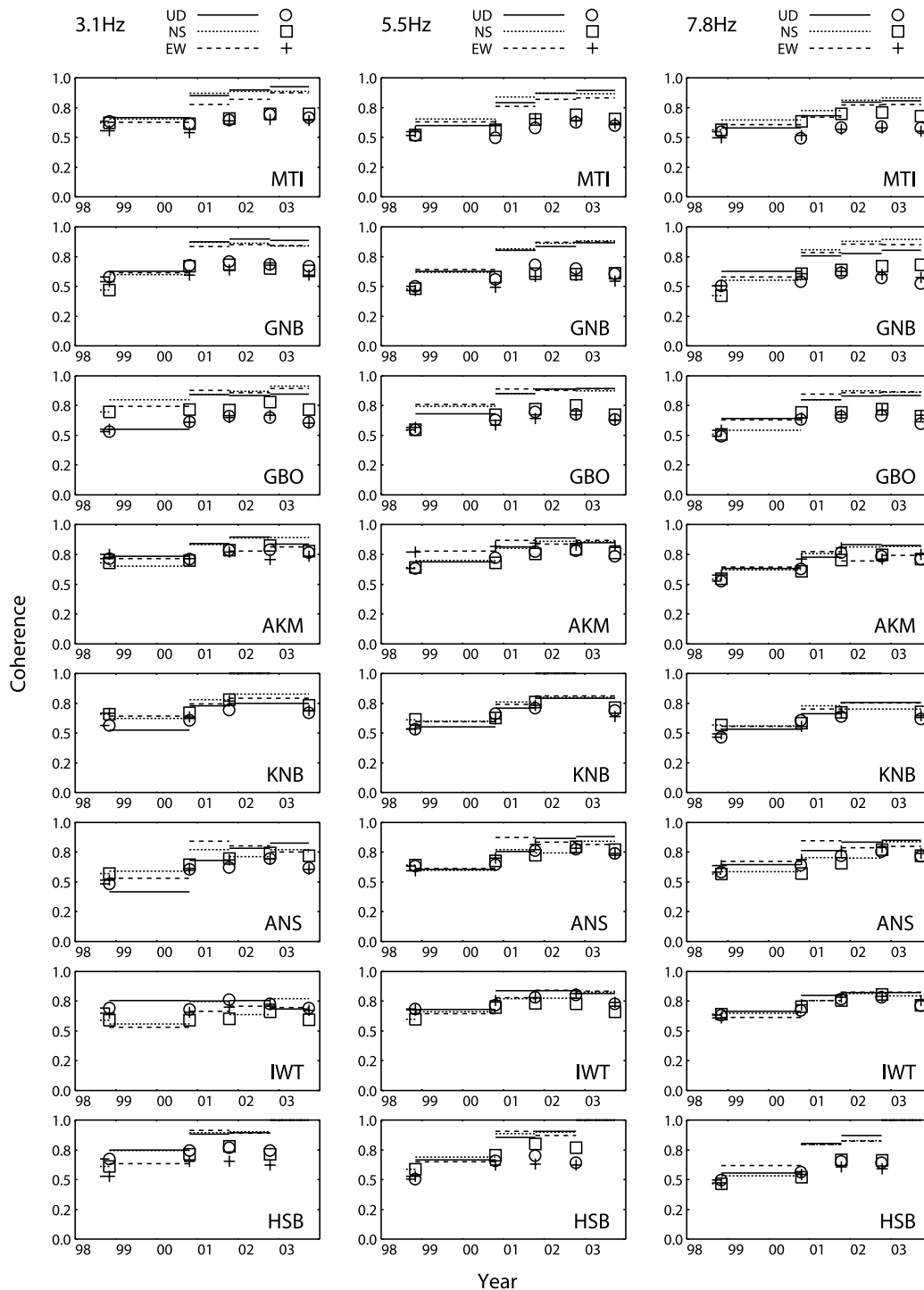
Fig. 9. Temporal variations of the coherence at 3.1, 5.5 and 7.8 Hz. The coherences are calculated for a time window of 10 s from the beginning of *P*-wave. Open, square and plus symbols represent the coherences of UD, NS, and EW components, respectively, for the data pairs of shot 1 to the other shots. Horizontal lines represent the coherences for the pairs of consecutive shots.

quency of seismic waves.

Figure 6 shows temporal variations of the phase changes at 4.7 Hz from 1998 to 2003. At MTI, GNB and GBO stations, which are closely located at the northern parts of the M6.1 fault and the spherical volumetric sources (Miura *et al.*, 2000; Tohoku Univ., 2003), large changes over 10 deg/s (a positive value means an increase of $d\phi/dt$, i.e., velocity decrease) are found for the pair of shot 1–2. For the pairs of shot 1–3, shot 1–4 and shot 1–5, the phase changes for

each component gradually decrease with small fluctuations. However, for the pair of shot 1–6, the phase changes increase again. Most of the other stations show similar trends, but amplitudes of the phase changes are relatively small.

In Fig. 6, the phase changes estimated from the pairs consisting of consecutive shots (shot 1–2, shot 2–3, shot 3–4, shot 4–5, shot 5–6) are also indicated by horizontal bars (note that the horizontal lines for shot 1–2 are superimposed on the open circles, squares and plus symbols for shot 1–2).

The right and left ends of each horizontal bar indicate the times of the consecutive two shots, and the length of the vertical lines at the ends represent one standard deviation. For shot 2–3, the phase changes are distributed around zero at most of the stations (MTI, KNB, ABO, AKM, HSB), and all data for shot 3–4 show negative phase changes. The phase changes are distributed around zero for shot 4–5 and increase again for shot 5–6. These trends are consistent with the overall features of the results obtained for the pairs of shot 1 to the others: increases of phase changes for shot 1–2 are gradually recovered by the time of shot 5, and then, small increases are observed again for shot 5–6.

Figure 7 represents temporal variations of the phase change at 8.6 Hz. The characteristics are similar to those at 4.7 Hz, although amplitudes of the changes are smaller compared with the results at 4.7 Hz. It is also recognized that no significant increase is observed at GBO for shot 1–2 while GNB, which is located at the surface above GBO, indicates a positive phase change. This may imply that shallow surface structure at this station has different frequency dependence from the structure below.

We calculate the phase changes by using a short time window of 5 s to examine the difference of the wave type (body and surface waves) and the effect of the target region where the wave propagate through. The results show similar characteristics found in the results obtained from analyses using a 10 s time window (not shown in figure). Although a large difference is recognized in the result of GBO for shot 1–2 (the estimated phase change shows a negative value), accuracy of the estimation is not sufficient to discuss the difference in detail.

4.2   Velocity change

Although it is better to examine the temporal variation of the phase change at all of the frequency range, evaluation of all of the observed phase changes at once is not easy. In the present study, therefore, we estimate seismic velocity changes of the crust at a low frequency range (3–6 Hz) from the linear frequency dependence found in the phase changes. The velocity changes are calculated from the relation of $\Delta V/V = (2\pi f)d\phi/dt$, where f is the frequency of the waves and V the averaged velocity in the medium where scattered seismic waves propagate, respectively (Poupinet *et al.*, 1984; Nishimura *et al.*, 2000b). The best fit lines are indicated by a fine line in Fig. 5, and the estimated velocity changes, $\Delta V/V$, are shown at the bottom right of each panel. Temporal variations of the velocity changes from 1998 to 2003 are shown in Fig. 8. At MTI, GNB, GBO and KNB stations, a large amount of velocity reduction (over -0.5%) is found for the pair of shot 1–2. The velocity changes at GNB and GBO are estimated to be -0.93% and -0.88%, respectively. The velocity changes at these stations gradually increase for shot 1–3, and reach about -0.6% for shot 1–5. However, a slight decrease of 0.1–0.2% in the velocity change is observed again for shot-1–6. Most of the other stations show the trends similar to GNB and GBO stations, although the velocity changes estimated at MTI and AKM stations decreased for shot 1–3 (The changes for shot 1–3 are about 0.1–0.2% smaller than those for shot 1–2).
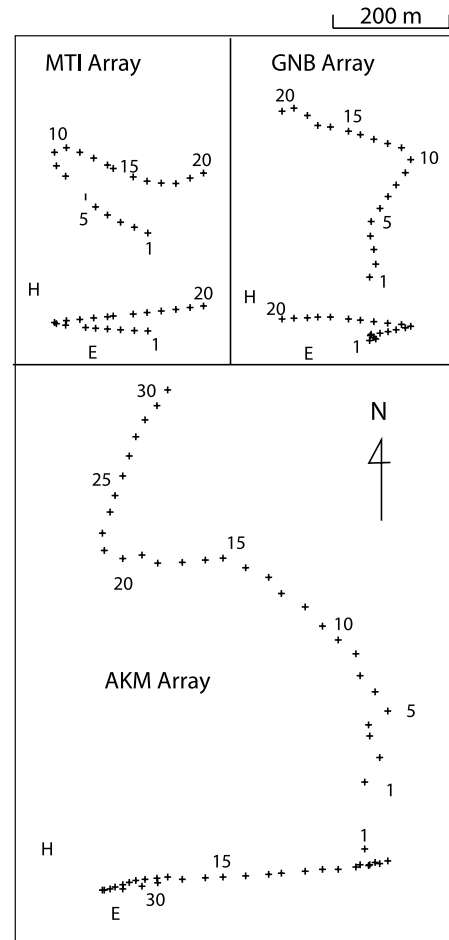

Fig. 10.   Configuration of seismic arrays (plus marks) at MTI, GNB, and AKM stations. Map view and vertical cross section in the E-W direction are shown in the upper and lower parts, respectively. Scales and direction of all panels are same.

4.3   Coherence

Figure 9 represents temporal variations of the coherence for the eight stations at 3.1 Hz, 5.5 Hz and 7.6 Hz. The coherences are estimated from the waveform for a 10 s time window beginning from P-wave arrivals. The coherences for the pairs of consecutive shots are large compared with those for the pair of shot 1 to the other. This result could be plausible enough if the crustal structure gradually changes with time. It is also found that the coherences gradually increase from shot 1–2 to the other pairs with time. These characteristics are qualitatively consistent with the coherence recovery that is reported for waveform analyses of multiplet earthquakes related to the M6.9 Loma Prieta Earthquake (Baish and Bokelmann, 2001). However, in our experiments, all of the stations show similar temporal tendency in the coherence, and the shot points are located on the M6.1 fault. So, we cannot distinguish which the main origin of the temporal variations in coherence is, the crustal structure or the seismic source.

5.   Semblance Analysis of Seismic Arrays

We examine the wave properties of the observed seismic waves by analyzing seismic array data. Figure 10 shows three seismic arrays deployed around MTI, GNB and AKM
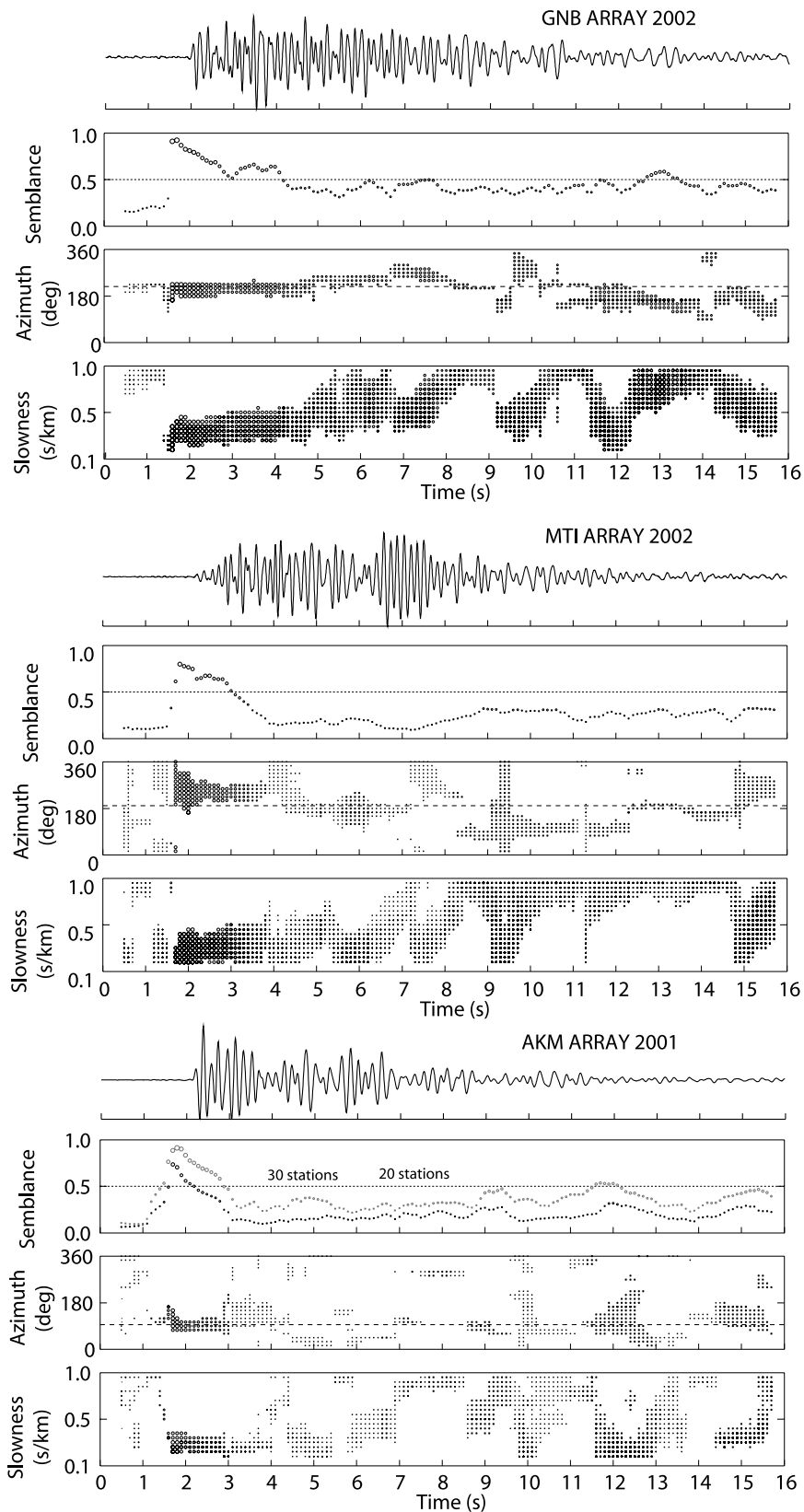
Fig. 11.   Time sequences of the semblance, incident azimuth and slowness of the seismic waves observed at the MTI, GNB, and AKM arrays. Sizes of open circles are proportional to the semblance coefficients. Gray circles in semblance for AKM arrays are the results estimated from 20 seismic stations (no. 10–30 in Fig. 10).

stations. Each of the MTI and GNB arrays consisted of 20 vertical components of short-period (0.5 s) seismometers and recorded the signals from the shots 4 and 5. The AKM array had 30 short-period (0.5 s) seismometers to record the seismic waves excited by the shot 4. Signals from each short-period seismometer were digitized with a sampling
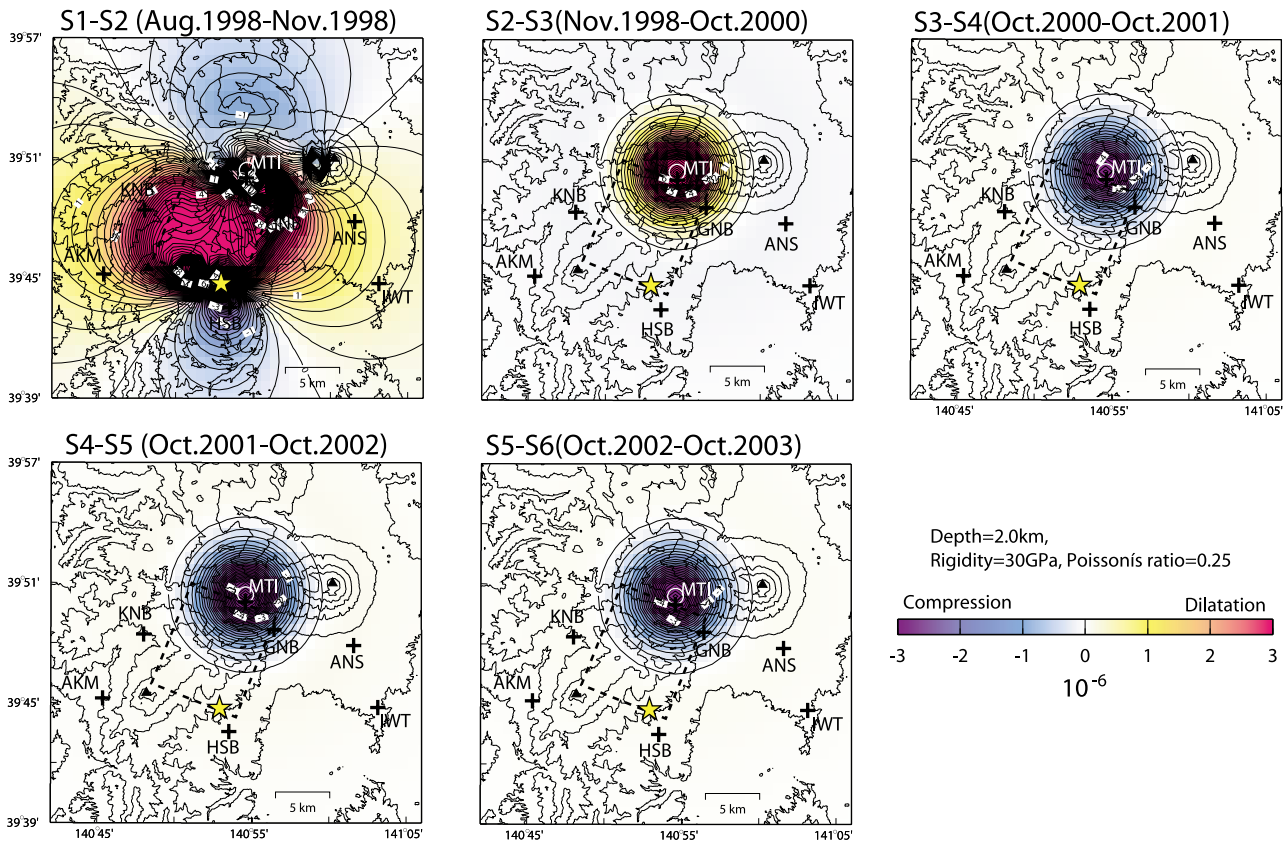
Fig. 12.   Spatio-temporal changes of volumetric strains around the M6.1 fault (rectangular of broken lines) and Iwate volcano for the period of shots 1–2, 2–3, 3–4, 4–5, and 5–6. Results at 2.0 km depth are plotted. Red and blue colors represent dilatation and compression, respectively. Contour interval is 0.2 micro strain. Shot point and seismic stations are represented by a star and plus symbols, respectively.

frequency of 250 Hz and an A/D resolution of 16–24 bits by portable data recorders (LS8000SH of Hakusan Co. for GNB and MTI; LS7000 of Hakusan Co. for AKM). The clock of each data logger was corrected by GPS signals just before each explosion, so that the sampling difference between stations were negligibly small (<1 ms).

We apply a semblance method (Neidell and Taner, 1971) to these seismic array data to clarify the wave property. For each array data set, semblance, slowness, and incident azimuth as a function of time are calculated at the frequency of 3–6 Hz by shifting a time window every 0.1 s from the beginning. Length of the time window is set at 1 s. Height correction of each seismometer is made by assuming a surface structure with a velocity of 2.0 km/s. Figure 11 shows time functions of the maximum semblance coefficients obtained for each time window. Results of the MTI and GNB arrays are shown for the data of shot 5. Slowness and azimuth of the wave whose semblance coefficient is more than 90% of the maximum semblance coefficient for each time window are plotted. For the GNB array, large semblance coefficients are observed for the P-wave that is followed by coda waves having semblance coefficients larger than 0.4. The incident azimuth of the P-wave is consistent with the back azimuth (216 deg), and the slowness of P-wave is estimated to be 0.2–0.4 s/km. The incident azimuth does not change for about 3 s beginning from the P-wave arrival. After the S-wave arrival, the incident azimuth seems to slightly shift to the south-west (azimuth is about 240 deg), and the slow-

ness tends to become larger (0.3–1.0 s/km). The beginning time of the change (about 4.8 s in Fig. 11) is later than or almost same with the time when a large bump is observed in the phase difference (see at about 3.8 s of shots 1–2 and 1–6 in Fig. 4(b)). For the waves later than 10 s, the incident azimuth gradually shifts to the south-east (azimuth is about 150 deg), and the slowness sometimes reaches 1.0 s/km. These results suggest that the seismic waves observed at GNB station are incident mainly from the direction of the shot point and that the former part of the waves mainly consists of P and S-waves while the latter is surface waves. For the MTI and AKM arrays, the semblance coefficients indicate large values of more than 0.5 for about 1 s after direct P-wave. But, the semblance coefficients rapidly decrease with time, and reach low values less than 0.4. These low semblance coefficients suggest that the coda waves are incoherently incident from various directions to these stations and/or that surface structures beneath these arrays are much heterogeneous. This is contrary to the coda waves observed at the GNB array. Such low semblance coefficients may be attributable to difference in total numbers of seismometers used at each array or difference of spatial intervals of seismic stations (25 m, 24 m, and 36 m for MTI, GNB, and AKM arrays, respectively). However, even when only two third of the seismometers at the AKM arrays are used for semblance analyses (no. 11 to 30 in Fig. 10 are used), we obtain low-semblance coefficients. And also, semblance coefficients at a low frequency band of 2–4 Hz, which may

decrease the effect of spatial intervals of the seismometers, show similar features in the MTI and AKM arrays. These observations imply that the low semblance coefficients observed at the AKM and MTI arrays are not caused from seismic array configurations.

The observed incident azimuth of the *P*-wave at the AKM array is almost consistent with the geometrical back azimuth, but that of the MTI array shifts about 45 degree west of the back azimuth. This inconsistency found at the MTI array seems to originate from height difference of the station locations, and may be improved if we use appropriate seismic velocity beneath the arrays. But the difference does not affect the following discussion.

We calculate semblance coefficients for the shot 4 data of the GNB and MTI arrays, and the results are quite similar to those mentioned above.

6. Discussion
6.1 Comparison of seismic velocity changes with spatio-temporal changes in volumetric strains around the M6.1 fault and Iwate volcano

By using the M6.1 fault model of Miura *et al.* (2000) and the spatio-temporal distributions of the volcanic pressure sources from 1998 to 2002 by Tohoku Univ. (2003), we calculate volumetric strains around the M6.1 fault and Iwate volcano. We further estimate volumetric strains in 2003 by analyzing the geodetic data with same method. Figure 12 shows spatial distributions of the volumetric strain at a depth of 2 km for the period from 1998 to 2003. Red and blue colors denote dilatation and compression, respectively. For the period from August 1998 to November 1998 (shot 1–2), the M6.1 earthquake took place to release the stress, and the volcanic pressure sources inflated the western part of Iwate volcano. As a result, dilatation in the crustal structure is observed mainly at the eastern and western regions of the fault while compression is caused at the south of the fault and the north of the volcano. It is found that the stations indicating large amplitude of velocity decreases (GNB, GBO, MTI) are near to strongly dilated regions. For the period from November 1998 to 2000 (shot 2–3), only the spherical volumetric source was active. Accordingly, the dilated regions are concentrated at the western part of the volcano where MTI and GNB stations are located at. For the periods from 2000 to 2002 (shots 3–5), the spatial distributions of the volumetric strains are almost same except that the polarity is reversed from dilatation to compression; the stations close to the western part of the volcano (MTI and GNB) are located on the compression regions while the other stations are on slightly dilated regions. In these periods (shot 2–5), slight increases of the velocity changes are observed at most of the stations. From 2002 to 2003, small decreases are detected again at most of the stations. These decreases may be attributed to a small seismic swarm accompanying a small crustal deformation occurred at the northern flank of Akita-Komagatake volcano during June 2003 (Ueki *et al.*, 2004). However, the activity was too small to change the tendency of the spatial distribution of the volumetric strains beginning from 2000.

The velocity changes observed for shot 1–2 are well matched with the spatial patterns of the volumetric strain.

However, the velocity changes observed for the following period are not completely matched with the predicted volumetric strains. This is probably because the strain changes observed after shot 2 are quite small in amplitude for most of the stations except MTI and GNB stations. As for GNB station, the coda waves always come from the structure beneath the M6.1 fault which show a weak compression at shallow parts. Hence, the detected velocity changes come to be not so affected by the deformation field close to the spherical volumetric sources. And also, the calculated deformation field may not include the regional stress, which is caused by, for example, the Pacific plate motion that compresses the Tohoku District in E-W direction (Miura *et al.*, 2002) because the geodetic measurements (Miura *et al.*, 2000; Tohoku Univ., 2003) were concentrated around Iwate volcano.

6.2 Sensitivity of velocity change to stress loading

So far, we have qualitatively compared the velocity changes with the strain field around the M6.1 fault and Iwate volcano. Although it is not easy to exactly know where the coda waves observed at each station propagate in the crust, we suppose in the present study that the coda waves mainly consist of the waves propagating in a region surrounded by a scattering shell (e.g., Sato and Fehler, 1998). Location of the scattering shell (x, y, z) can be determined from the location of station and shot point, lapse time, and an effective seismic velocity, which satisfy the following equation:

$$\sqrt{(x - x_s)^2 + (y - y_s)^2 + (z - z_s)^2} \\ + \sqrt{(x - x_e)^2 + (y - y_e)^2 + (z - z_e)^2} = V_e T \quad (1)$$

where x_s, y_s, z_s are the location of station, x_e, y_e, z_e are the location of shot point, is the effective seismic velocity and T is the lapse time. Large effective velocity implies that coda waves propagate in a large volume and arrive at the station from various directions. On the other hand, small effective velocity suggests that coda waves mainly come from a direction of the source, as is observed at the GNB array, so that the scattering shell becomes small. This may be interpreted as that the former case is a representation that single scattering is dominant and/or the coda waves mainly consist of body waves, whereas the latter case corresponds to that multiply scattered waves and/or surface waves are dominant in the coda waves.

First, we tentatively assume the effective velocity to calculate an average of the volumetric strain in the region enclosed by a scattering shell. Then, we fit a straight line to the relation between the average volumetric strains and the seismic velocity changes obtained for consecutive shots, and then we calculate the residuals between the predicted and observed relations for each station. We calculate the residuals for the effective velocity ranging from 1.2 km/s to 2.2 km/s to select the best effective velocity that has the minimum residuals. Figure 13 compares the average volumetric strains with the observed seismic velocity changes at 3–6 Hz (Fig. 8) for each station. The best fit lines determined from least square method are illustrated by solid lines, and the effective velocities are shown at the top of the right in each panel. The slopes of the best fit lines indicate strain

Table 2. Theoretical volumetric strains in the crust due to tidal loading at the time of the six artificial explosions. Volumetric strains are calculated by using GOTIC2 program (Matsumoto, K. *et al.*, 2001).

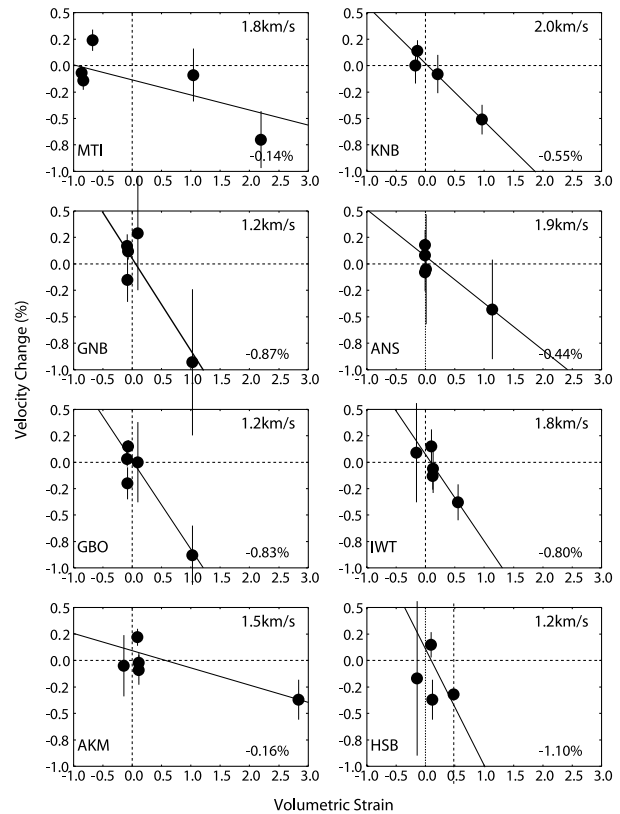| Shot	Volumetric Strain
S1	5.1466e-09
S2	8.0070e-09
S3	1.2091e-08
S4	−7.1959e-09
S5	2.1670e-08
S6	2.5960e-10
S2–S1	2.8604e-09
S3–S2	4.0843e-09
S4–S3	−1.9287e-08
S5–S4	2.8866e-08
S6–S5	−2.1410e-08

Fig. 13. Comparison of the average volumetric strains with the observed seismic velocity changes. The data are shown by solid circles with error bars (one standard deviation). Unit of horizontal axis is micro strain. Solid lines represent the best fit lines estimated by least squares method. The effective seismic velocity in km/s and the strain sensitivity of velocity change (km/s/micro strain in percentage) are shown on the top right and bottom right in each panel indicate, respectively.

sensitivities of the seismic velocity change, $1/V\,(dV/d\epsilon)$, where ϵ is the volumetric strain. For the eight stations, the strain sensitivity is estimated to be −0.0014 to −0.011 / micro strain, most of which are ranging from −0.004 to −0.008/micro strain. Assuming a bulk modulus of 5×10^{10} Pa, we estimate the stress sensitivity of the velocity change, $1/V\,(dV/d\sigma)$, to be 0.03 to 0.2 /MPa, where σ is the stress. The effective seismic velocities are estimated to be 1.2 km/s for GNB and GBO stations, while 1.8 km/s and 1.5 km/s for MTI and AKM stations. Since smaller effective seismic velocity reflects a small scattering shell, these results are consistent with the results obtained from our semblance analyses.

So far, the seismic velocity changes at the low frequency of 3–6 Hz have been discussed. Since the observed phase changes at the high frequency (6–9 Hz) are equal to or smaller than those at the lower frequency (3–6 Hz), the stress sensitivities at 6–9 Hz come to be smaller than 0.03–0.2 /MPa.

6.3   Effect of tidal loading

Seismic velocity changes of the crust have been often discussed in terms of temporal changes of the stress field caused by the tidal loadings. Reasenberg and Aki (1974) estimated the stress sensitivity of velocity change in the rock to be 2.0 /MPa from analyses of the seismic wave (probably Rayleigh wave of about 30 Hz) propagating over a distance of 200 m. Recently, Yamamura *et al.* (2003) accurately estimated the pressure sensitivity of P-wave velocity at about 100 Hz in natural rocks to be 0.5 /MPa from a 1-year continuous measurement of rocks across a distance of 12 m in a vault by using a piezoelectric transducer. Furumoto *et al.* (2001) also obtained 1 /MPa for the pressure sensitivity of velocity changes in the crust from the arrival time data of initial phase (P-wave) of 10-years artificial explosions at stations in Tokai area, Japan. As summarized in table 1 of Yamamura *et al.* (2003), the stress sensitivities of velocity change are ranging from 5×10^{-3} to 2 /MPa. It is noted that these sensitivities are obtained at different fields, different frequency bands and/or different wave types. Table 2 shows volumetric strains at the south of Iwate volcano due to the tidal loading for shots 1–6, which are calculated by

the GOTIC2 program (Matsumoto, K. *et al.*, 2001). Differences of the volumetric strains between each pair of two shots are ranging from -2.1×10^{-8} to 2.9×10^{-8} so that the stress difference are estimated to be from -1.1×10^{3} Pa to 1.4×10^{3} Pa on the assumption of a bulk modulus of 5×10^{10} Pa. If we assume a pressure sensitivity of 0.2 /MPa, the velocity changes caused by the tidal strains are estimated to be less than ±0.02%. Even if we use 1 /MPa, the tidal effects are too small to drastically change the observed temporal variations in the velocity change shown in Fig. 8.

6.4   Origins of the velocity changes in crustal structure

Recent seismic researches have shown remarkable temporal changes of the crustal structure associated with a large earthquake occurrence. For example, repeated seismic surveys of the 1992 M7.5 Landers earthquake show seismic velocity increase of about 0.5 to 1.5% from 1994 to 1996 (Li *et al.*, 1998). Coherence analyses of multiplet events indicate a recovery of the structural changes caused by the 1989 M6.9 Loma Prieta earthquake in about 5 years. S-wave splitting observed at stations closely located to Nojima fault, Japan, suggest a fault healing within 33 months after the occurrence of the 1995 M7.2 Hyogo-ken Nanbu earthquake (Tadokoro and Ando, 2002). These studies attribute the origins of structural changes to crack opening and closure in the crust due to stress loading. Changes of

water condition in the crust may be another candidate for the case of Iwate volcano. For example, as water-saturated rock changes its internal condition from vapor-saturated to liquid-saturated, the compressional velocity increases and shear wave velocity decreases (Ito *et al.*, 1979). At the Geyser geothermal site, temporal changes of Vp and Vs measured by 4D tomography are explained by water depletion process (Gunasekera *et al.*, 2003). Especially at MTI, GNB, and GBO stations, the observed velocity changes might have been caused by hot-waters induced by the volcanic pressure sources. However, seismic velocity changes are widely detected at the other stations such as AKM and IWT, which are far from the volcanic pressure sources of Iwate volcano. Therefore, we infer that the main origins of the observed velocity changes are caused from the stress changes, which may be related with crack openings and closure in the crust.

The recovery rate of crustal structure around Iwate volcano is smaller than those of the Landers, Loma Prieta, and Hyogo-ken Nanbu earthquakes. While these regions have almost completed the recovery within a few to 5 years, only less than a half of the velocity changes has been recovered around the M6.1 fault for the five years (e.g., −0.9% to −0.6% for GNB station). Such slow recovery may reflect regional deformation fields at the target fields. For example, geodetic data collected during the past 100 years shows that the Tohoku district, in which Iwate volcano is located, is under extension (Ishikawa and Hashimoto, 1999). On the other hand, the shear strain rate deduced from the recent GPS measurement indicate that Hyogo-ken Nanbu earthquake is placed on a strong deformation field called as the Niigata-Kobe Tectonic Zone (Sagiya *et al.*, 2000). Such difference in strain rates suggests that the recovery of the crustal structure is controlled by the stress condition around the target region. However, as pointed out by Ishikawa and Hashimoto (1999), it is necessary to note that the deformation field obtained from the 100 years data is not matched with that by recent GPS measurements at several areas. Crack orientations may another candidate to control the recovery process, as Tadokoro and Ando (2002) recently attributed fault healing process to crack closure due to regional stress at Hyogo-ken Nanbu earthquake. When crack orientation is perpendicular to the maximal strain axis, crack closures are expected to be delayed.

One of the most important results in the present study is the frequency dependence found in the velocity change (fractional change of seismic velocity). Similar frequency dependence on temporal change of seismic wave is reported in coda Q analyses. Sato *et al.* (1988b) reported that $\log(Q_c^{-1} f)$ at frequency of 5 Hz took lower value in the three-year period preceding the $M_L = 5.2$ earthquake at Garum, Central Asia, while such changes are not so well recognized at higher frequency ranges. Sato (1988a) summarized that temporal changes are often found in the waves at low frequency range (2–6 Hz), and Baish and Bokelmann (2001) mentioned that coherency changes in seismic waves seem to be significant at lower frequency range of less than 8 Hz. These results and our result strongly suggest an existence of frequency dependent characteristics in fractional changes of the seismic wave velocity in the crust.

7. Summary

We have shown remarkable temporal changes in the seismic velocity of the crust around the M6.1 fault and Iwate volcano, by measuring the phase difference in the seismic waves excited by six artificial explosions. The seismic velocity of the crust decreased by about 1% in 1998, and the origins are considered to be dilatation in the crust which is caused by the M6.1 earthquake and the volcanic pressure sources of Iwate volcano. About one third of the reduction in seismic velocity is gradually recovered by the middle of 2002, but seismic velocity decrease is observed again in 2003. Volumetric strain fields predicted for these periods are not completely matched with the velocity changes, although regional tectonic stress field may explain the inconsistency. It should be noted that the observed fractional changes in the seismic velocity indicate frequency dependent characteristics: the velocity changes are almost constant at the low frequency range (3–6 Hz) while the magnitude of the velocity changes decreases with frequency at the high frequency range (6–9 Hz).

References

Baish, S. and G. H. R. Bokelmann, Seismic waveform attributes before and after the Loma Prieta earthquake: Scattering change near the earthquake and temporal recovery, *J. Geophys. Res.*, **106**, 16323–16337, 2001.

Doi, N., Change of surface volcanic phenomena at the West Iwate volcano from march, 1999 to May, 2001, Report of Coordinating Committee for Prediction of Volcanic Eruptions, 79, 44–48, 2002 (in Japanese).

Earthquake Information Center, University of Tokyo, EIC Seismological Note, No. 50, 1998 (in Japanese).

Furumoto, M., Y. Ichimori, N. Hayashi, and Y. Hiramatsu, Seismic wave velocity changes and stress build-up in the crust of the Kanto-Tokai region, *Geophys. Res. Lett.*, **28**, 3737–3740, 2001.

Geographical Survey Institute, Crustal deformations of Mt. Iwate and its surrounding area, Report of Coordinating Committee for Prediction of Volcanic Eruptions, 82, 17–20, 2003 (in Japanese).

Gunasekera, R. C., G. R. Foulger, and B. R. Julian, Reservoir depletion at the Geysers geothermal area, California, shown by four-dimensional seismic tomography, *J. Geophys. Res.*, **108**, doi:10.1029/2001JB000638, 2003.

Hiramatsu, Y., N. Hayashi, M. Furumoto, and H. Katao, Temporal chages in coda Q-1 and b value due to the static stress change associated with the 1995 Hyogo-ken Nanbu earthquake, *J. Geophys. Res.*, **105**, 6141–6151, 2000.

Ishikawa, N. and M. Hashimoto, Average horizontal crustal strain rates in Japan during interseismic period deduced from geodetic surveys (Part 2), *Bull. Seism. Soc. Jpn*, **52**, 299–315, 1999 (in Japanese with English abstract).

Ito, H., J. D. Vilbiss, and A. Nur, Compressional and shear waves in saturated rock during water-steam transition, *J. Geophys. Res.*, **84**, 4731–4735, 1979.

Koshiya, S. and M. Ohtani, Earthquake fault of the M6.1 earthquakes occurred at the northern part of Iwate Prefecture on September 3, 1998,

Chikyu, **21**, 307–311, 1999 (in Japanese).

Li, Y. G., J. E. Vidale, K. Aki, F. Xu, and T. Burdette, Evidence of shallow fault zone strengthening after the 1992 M7.5 Landers, California, earthquake, *Science*, **279**, 217–219, 1998.

Matsumoto, K., T. Sato, T. Takanezawa, and M. Ooe, GOTIC2: A program for computation of oceanic tidal loading effect, *J. Geod. Soc. Japan*, **47**, 243–248, 2001.

Matsumoto, S., K. Obara, K. Yoshimoto, T. Saito, A. Ito, and A. Hasegawa, Temporal change in P-wave scatterer distribution associated with the M6.1 earthquake near Iwate volcano, northeastern Japan, *Geophys. J. Int.*, **145**, 48–58, 2001.

Matsushima, J., T. Yokota, Y. Okubo, S. Rokugawa, K. Tanaka, T. Tsuchiya, N. Narita, and K. Tani, Repeated seismic reflection measurements in the Kakkonda geothermal field, *J. Volcanol. Geotherm. Res.*, **129**, 343–356, 2004.

Miura, S., S. Ueki, T. Sato, K. Tachibana, and H. Hamaguchi, Crustal deformation associated with the 1998 seismo-volcanic crisis of Iwate Volcano, Northeastern Japan, as observed by a dense GPS network, *Earth Planets Space*, **52**, 1003–1008, 2000.

Miura, S., T. Sato, K. Tachibana, Y. Satake, and A. Hasegawa, Strain accumulation in and around Ou Backboe Range, northeastern Japan as observed by a dense GPS network, *Earth Planets Space*, **54**, 1071–1076, 2002.

Nakahara, H., T. Nishimura, H. Sato, M. Ohtake, S. Kinoshita, and H. Hamaguchi, Broad-band source process of the 1998 Iwate Prefecture, Japan, earthquakes as revealed from inversion analyses of seismic waveforms and envelopes, *Bull. Soc. Seismol. Am.*, **92**, 1708–1720, 2002.

Nakamichi, H., H. Hamaguchi, S. Tanaka, S. Ueki, T. Nishimura, and A. Hasegawa, Source mechanisms of deep and intermediate-depth low-frequency earthquakes beneath Iwate volcano, northeastern Japan, *Geophys. J. Int.*, **154**, 811–828, 2003.

Nakamura, A., A. Hasegawa, N. Hirata, T. Iwasaki, and H. Hamaguchi, Temporal variations of seismic wave velocity associated with 1998 M6.1 Shizukuishi earthquake, *Pure. Appl. Geophys.*, **159**, 1183–1204, 2002.

Neidell, N. S. and M. T. Taner, Semblance and other coherency measures for multi-channel data, *Geophysics*, **36**, 482–497, 1971.

Nishimura, T., H. Nakamichi, S. Tanaka, M. Sato, T. Kobayashi, S. Ueki, H. Hamaguchi, M. Ohtake, and H. Sato, Source process of very long period seismic events associated with the 1998 activity of Iwate Volcano, northeastern Japan, *J. Geophys. Res.*, **105**, 19135–19147, 2000a.

Nishimura, T., N. Uchida, H. Sato, M. Ohtake, S. Tanaka, and H. Hamaguchi, Temporal changes of the crustal structure associated with the M6.1 earthquake on September 3, 1998, and the volcanic activity of Mount Iwate, Japan, *Geophys. Res. Lett.*, **27**, 269–272, 2000b.

Poupinet, G., W. L. Ellsworth, and J. Frechet, Monitoring velocity variations in the crust using earthquake doublets: An application to the Calaveras fault, California, *J. Geophys. Res.*, **89**, 5719–5731, 1984.

Poupinet, G., G. A. Ratdomopurbo, and O. Coutant, On the use of earthquake multiplets to study fractures and the temporal evolution of an active volcano, *Annali di Geophysica*, **36**, 253–264, 1996.

Ratdomopurbo, A. and G. Poupinet, Monitoring a temporal change of seismic velocity in a volcano: application to the 1992 eruption of Mt. Merapi (Indonesia), *Geophys. Res. Lett.*, **22**, 775–778, 1995.

Reasenberg, P. and K. Aki, A precise, continuous measurement of seismic velocity for monitoring in situ stress, *J. Geophys. Res.*, **79**, 399–406, 1974.

Sagiya, T., S. Miyazaki, and T. Tada, Continuous GPS array and present-day crustal deformation of Japan, *Pure Appl. Geophys.*, **157**, 2303–2322, 2000.

Saiga, A., Y. Hiramatsu, T. Ooida, and K. Yamaoka, Spatial variation in the crustal anisotropy and its temporal variation associated with a moderate-sized earthquake in the Tokai region, central Japan, *Geophys. J. Int.*, **154**, 695–705, 2003.

Sato, H., Temporal change in scattering and attenuation associated with the earthquake occurrence—A review of recent studies on coda waves, *PAGEOPH*, **126**, 465–497, 1988a.

Sato, H., A. M. Shomahmadov, V. I. Khalturin, and T. G. Rautian, Temporal changes in spectral coda attenuation Qc-1 associated with the K=13.3 earthquake of 1983 near Garum, Tadjikistan region in Soviet Central Asia, *Bull. Seismo. Soc. Jpn.*, **41**, 39–46, 1988b (in Japanese with English abstract).

Sato, H. and M. Fehler, *Seismic Wave Propagation and Scattering in the Heterogeneous Earth*, AIP Press/Springer-Verlag, New York, pp. 308, 1998.

Tadokoro, K. and M. Ando, Evidence for rapid fault healing derived from temporal changes in S wave splitting, *Geophys. Res. Lett.*, **29**, 10.1029/2001GL013644, 2002.

Tanaka, S., H. Hamaguchi, T. Nishimura, T. Yamawaki, S. Ueki, H. Nakamichi, T et al., Three-dimensional P-wave velocity structure of Iwate volcano, Japan from active seismic survey, *Geophys. Res. Lett.*, **29**, 10.1029/2002GL014983, 2002a.

Tanaka, S., H. Hamaguchi, S. Ueki, M. Sato, and H. Nakamichi, Migration of seismic activity during the 1998 volcanic unrest at Iwate volcano, northeastern Japan, with reference to P and S wave velocity anomaly and crustal deformation, *J. Volcanol. Geotherm. Res.*, **113**, 399–414, 2002b.

Tohoku Univ., Seismic activity and crustal deformation at Iwate Volcano in the period from June 2001 to September 2002, Report of Coordinating Committee for Prediction of Volcanic Eruptions, 83, 6–13, 2003 (in Japanese).

Uchida, N., T. Nishimura, K. Yoshimoto, H. Nakahara, H. Sato, M. Ohtake, S. Tanaka, and H. Hamaguchi, Temporal change of seismic-wave velocity associated with the 1998 northern Iwate prefecture, Japan, earthquake, *Bull. Seism. Soc. Jpn.*, **55**, 193–206, 2002 (in Japanese with English abstract).

Ueki, S., S. Tanaka, and M. Sato, Seismic activity and crustal deformation in and around Akita-komagatake and Iwate volcanoes, possibly triggered by Off-Miyagi EQ, Abstracts 2004 Japan Earth and Planetary Science Joint Meeting, V055-011, 2004.

Umino, N., T. Okada, A. Nakamura, J. Nakajima, T. Sato, S. Hori, T. Kono, K. Nida, S. Ueki, T. Matsuzawa, A. Hasegawa, and H. Hamaguchi, Aftershock distribution for the M6.1 earthquake of 3 September 1998 in Shizukuishi, Iwate prefecture, northeastern Japan, *Active Fault Research*, **17**, 1–8, 1998 (in Japanese with English abstract).

Yamamura, K., O. Sano, H. Utada, Y. Takei, S. Nakao, and Y. Fukao, Long-term observation of in situ seismic velocity and attenuation, *J. Geophys. Res.*, **108**, doi:10.1029/2002JB002005, 2003.

T. Nishimura (e-mail: nishi@zisin.geophys.tohoku.ac.jp), S. Tanaka, T. Yamawaki, H. Yamamoto, T. Sano, M. Sato, H. Nakahara, N. Uchida, S. Hori, and H. Sato